ATLAS NOTE

ATLAS-CONF-2016-088

5th August 2016

Search for charged Higgs bosons in the τ+jets final state with 14.7 fb^{-1} of pp collision data recorded at $\sqrt{s}$ = 13 TeV with the ATLAS experiment

The ATLAS Collaboration

ATLAS-CONF-2016-088
08 August 2016

Abstract

The experimental observation of charged Higgs bosons, $H^{\pm}$, which are predicted by several models with an extended Higgs sector, would indicate physics beyond the Standard Model. This note presents the results of a search for charged Higgs bosons in 14.7 fb^{-1} of pp collision data at $\sqrt{s}$ = 13 TeV recorded by the ATLAS detector at the LHC. The search targets the τ+jets channel in top-quark-associated $H^{\pm}$ production with a hadronically decaying W boson and τ lepton in the final state. No evidence of a charged Higgs boson is found. For the mass range of $m_{H^{\pm}} = 200 - 2000$ GeV, upper limits are set on the production cross section of the charged Higgs boson with the subsequent decay $H^{\pm} \to \tau\nu$ in a range of 2.0 to 0.008 pb.

1 Introduction

Following the discovery of a neutral scalar particle at the Large Hadron Collider (LHC) in 2012 [1, 2], an important question is whether this new particle is the Higgs boson of the Standard Model (SM) or part of an extended Higgs sector. Charged Higgs bosons[1] appear in several non-minimal scalar sectors, where a second doublet [3] or triplets [4–8] are added to the SM Higgs doublet. In two-Higgs-doublet models (2HDM), the production and decay of the charged Higgs boson also depend on the parameter $\tan\beta$, defined as the ratio of the vacuum expectation values of the two Higgs doublets, and the mixing angle α between the two CP-even Higgs bosons. In the alignment limit, where $\cos(\beta-\alpha) \simeq 0$, the decay $H^+ \to \tau\nu$ can have a substantial branching fraction. In a type-II 2HDM, even when the decay $H^+ \to tb$ dominates, the branching fraction $\mathrm{BR}(H^+ \to \tau\nu)$ can reach 10–15% at large values of $\tan\beta$ [9]. Beyond tree level, a number of additional parameters affect the Higgs sector, the choice of which defines various MSSM benchmark scenarios. In some scenarios, such as $m_h^{\mathrm{mod+}}$ [10], the top-squark mixing parameter is chosen such that the mass of the lightest CP-even Higgs boson, m_h, is close to the measured mass of the Higgs boson that was discovered at the LHC. A different approach is employed in the hMSSM scenario [11, 12] in which the measured value of m_h can be used, with certain assumptions, to predict the remaining masses and couplings of the MSSM Higgs bosons without explicit reference to the soft supersymmetry-breaking parameters.

The ATLAS and CMS collaborations have searched for light charged Higgs bosons, produced in top-quark decays, using proton–proton (pp) collisions at $\sqrt{s}$ = 7–8 TeV in the $\tau\nu$ [13–17] and cs [18, 19] decay modes. Using data collected at $\sqrt{s}$ = 8 TeV, charged Higgs bosons heavier than the top quark were also searched for, using final states originating from both the $\tau\nu$ and tb decay modes [15, 17, 20]. The search for the $\tau\nu$ final states has been also performed by ATLAS at $\sqrt{s}$ = 13 TeV, using the data collected in 2015 [21]. Vector-boson-fusion H^+ production was also searched for by ATLAS using the WZ final state [22]. In parallel to this report, another search based on the data collected in 2015 and 2016, using the tb final states has been performed by ATLAS [23]. No evidence of a charged Higgs boson was found in any of these searches.

For m_{H^+} greater than the top-quark mass m_{top}, the main production mode of a charged Higgs boson at the LHC is expected to be in association with a top quark [24–26]. The corresponding Feynman diagrams are shown in Figure 1. When calculating the corresponding cross section in a four-flavour scheme (4FS), b-quarks are dynamically produced, whereas in a five-flavour scheme (5FS), the b-quark is also considered as an active flavour in the proton. 4FS and 5FS cross sections are averaged according to Ref. [27].

This note describes a search for charged Higgs bosons in pp collisions at $\sqrt{s}$ = 13 TeV using 14.7 fb^{-1} of data collected by the ATLAS experiment in 2015 and part of 2016. The production of a charged Higgs boson in association with a single top quark and its decay via $H^+ \to \tau\nu$ are explored in the mass range of 200 to 2000 GeV. This analysis uses the fully hadronic decay of the top quark ($t \to bW \to b(qq')$). The final state is characterised by the presence of a hadronic τ decay and missing transverse momentum arising from the H^+ decay, as well as the absence of high-transverse-momentum electrons and muons.

The SM prediction is compared to the data, and results for the signal cross section times branching fraction $\sigma(pp \to [b]tH^+) \times \mathrm{BR}(H^+ \to \tau\nu)$ are presented, together with an interpretation in the hMSSM benchmark scenario, in which the light CP-even Higgs boson mass m_h is set to 125 GeV, without choosing explicitly the soft-supersymmetry-breaking parameters.

[1] In the following, charged Higgs bosons are denoted H^+, with the charge-conjugate H^- always implied. Similarly, generic symbols are used for their decay products.

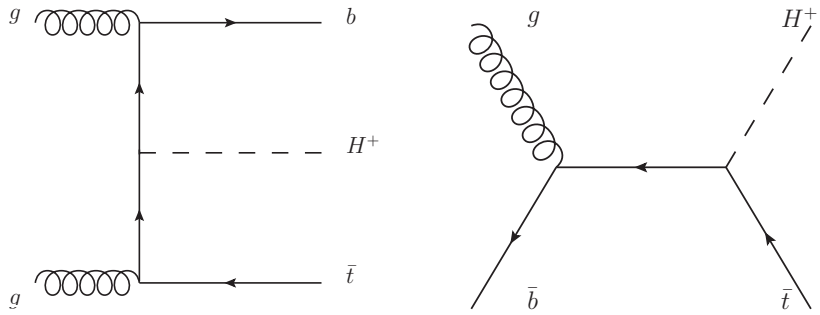

Figure 1: Leading-order Feynman diagrams for the production of a charged Higgs boson with a mass $m_{H^+} > m_{\text{top}}$, in association with a single top quark (left in the 4FS, and right in the 5FS).

2 Data and simulated events

The ATLAS experiment [28] consists of an inner detector with coverage in pseudorapidity[2] up to $|\eta| = 2.5$, surrounded by a thin 2 T superconducting solenoid, a calorimeter system extending up to $|\eta| = 4.9$ and a muon spectrometer extending up to $|\eta| = 2.7$ that measures the deflection of muon trajectories in the field of three superconducting toroid magnets. The innermost pixel layer, the insertable B-layer (IBL), was added between the first and second runs of the LHC, around a new, narrower and thinner beam pipe [29]. A two-level trigger system is used to select events of interest [30]. The integrated luminosity, considering the data-taking periods of 2015 and a fraction of 2016, in which all relevant detector subsystems were operational, is 14.7 fb^{-1} and has an uncertainty of 2.1% (3.7%) for data collected in 2015 (2016). It is derived following a methodology similar to that detailed in Ref. [31], from a calibration of the luminosity scale using x–y beam-separation scans performed in August 2015 and May 2016.

Simulated events of H^+ production in association with a single top quark are generated in the 4FS at the next-to-leading order (NLO) of QCD calculations with MadGraph5_aMC@NLO v.2.2.2 [32] using the NNPDF23LO [33] parton distribution function (PDF) set, interfaced to Pythia v8.186 [34] with the A14 set of tuned parameters (tune) [35] for the underlying event. For the signal generation, the QCD scale is set according to the latest theory recommendations [36] and reduces the signal acceptance with respect to the choice of $(m_{\text{top}} + m_{H^+})/3$ used in [21].[3] In the scenarios explored in this search, the width of H^+ is much smaller than the experimental transverse mass resolution, therefore the narrow-width approximation is used, which also allows to quote model-independent results.

The SM backgrounds are the production of $t\bar{t}$ pairs, single top quarks, W+jets, Z/γ^*+jets and electroweak gauge boson pairs ($WW/WZ/ZZ$), as well as multi-jet events. While $t\bar{t}$ production is the main background in the low mass search ($m_{H^+} \leq m_t$), multi-jet events dominate for the mass range considered in this search ($m_{H^+} > 200$ GeV). For the generation of $t\bar{t}$ pairs and single top quarks in the Wt- and s-channels, the Powheg-Box v2 [37, 38] generator with the CT10 [39, 40] PDF set in the matrix-element calculation is used. Electroweak t-channel single-top-quark events are generated using Powheg-Box v1. This generator uses the 4FS for the NLO matrix-element calculation together with the fixed four-flavour PDF set CT10F4.

[2] ATLAS uses a right-handed coordinate system with its origin at the nominal interaction point (IP) in the centre of the detector and the z-axis along the beam pipe. The x-axis points from the IP to the centre of the LHC ring, and the y-axis points upward. Cylindrical coordinates (r, ϕ) are used in the transverse plane, ϕ being the azimuthal angle around the z-axis. The pseudorapidity is defined in terms of the polar angle θ as $\eta = -\ln\tan(\theta/2)$.

[3] The acceptance reduction ranges from 22% for $m_{H^+} = 200$ GeV to <2.5% above 1000 GeV.

For this process, the top quark is decayed using MadSpin [41], thereby preserving all spin correlations. For all backgrounds above, the parton shower, the fragmentation and the underlying event are simulated using Pythia v6.428 [42] with the CTEQ6L1 [43] PDF set and the corresponding Perugia 2012 (P2012) tune [44]. The top-quark mass is set to 172.5 GeV for all relevant background and signal samples. The $t\bar{t}$ cross section is calculated at next-to-next-to-leading order (NNLO), including soft-gluon resummation to the next-to-next-to-leading logarithmic (NNLL) order, with Top++ v2.0 [45–51]. The single-top-quark samples are normalised to the approximate NNLO cross sections [52–54]. Events containing a W or Z boson with associated jets are simulated using MadGraph5_aMC@NLO v.2.2.2 at LO with the NNPDF23LO PDF set, interfaced to Pythia v8.186 with the A14 underlying-event tune. In these samples, Photos++ v3.52 [55] is employed for photon radiation from charged leptons. These samples are normalised to the NNLO cross sections calculated with FEWZ [56–58]. Finally, diboson processes are simulated using the Powheg-Box v2 generator interfaced to the Pythia v8.186 parton shower model. The CT10 NLO set is used as the PDF for the hard-scatter process, while the CTEQ6L1 PDF set is used for the parton shower. The AZNLO tune [59] is used for the QCD modelling. The diboson samples are normalised to their NLO cross sections, as computed by the event generator.

Simulation of b- and c-hadron decays is done with EvtGen v1.2.0 [60]. Multiple overlaid pp collisions (pile-up, with 20.5 collisions per bunch-crossing on average) are simulated with the soft QCD processes of Pythia v8.186 using the MSTW2008LO [61–63] PDF set and the A2 underlying-event tune [64]. All simulated signal and background samples are processed through a simulation [65] of the detector geometry and response using Geant4 [66]. Finally, they are processed through the same reconstruction software as the data. Simulated events are weighted to reproduce the same distribution of number of collisions per bunch crossing as observed in data.

Backgrounds are categorised based on the truth type of objects reconstructed as the visible decay products[4] of the hadronically decaying τ candidate ($\tau_{\text{had-vis}}$). Only the simulated events having a true hadronically decaying τ at generator level (τ_{had}) or with a charged lepton (electron or muon) misidentified as a $\tau_{\text{had-vis}}$ are kept. Backgrounds arising from a jet misidentified as a $\tau_{\text{had-vis}}$ candidate are estimated with a data-driven method.

3 Object reconstruction and identification

In the ATLAS experiment, hadronic jets are reconstructed from energy deposits in the calorimeters, using the anti-k_t algorithm [67] with a radius parameter $R = 0.4$. In the following, jets are required to have a transverse momentum $p_{\text{T}} > 25$ GeV and $|\eta| < 2.5$. A multi-variate technique (Jet Vertex Tagger) relying on jet energy and tracking variables to determine the likelihood that a given jet originates from pile-up [68] is applied to jets with $p_{\text{T}} < 60$ GeV and $|\eta| < 2.4$. Jets arising from b-hadron decays are identified using an algorithm that combines impact parameter information with the explicit identification of secondary and tertiary vertices within the jet into a b-tagging score [69, 70]. The minimal requirement imposed on the b-tagging score in this analysis corresponds to a 70% efficiency to tag a b-quark-initiated jet in $t\bar{t}$ events and rejection factor of about 400 for light-quark initiated jets. The tagging efficiencies from simulation are corrected based on the results of calibration performed with data [71].

[4] This refers to all τ decay products except the neutrinos.

Candidates for identification as $\tau_{\text{had-vis}}$ arise from jets that have $p_{\text{T}} > 10$ GeV and for which one or three charged-particle tracks are found within a cone of size[5] ΔR of 0.2 around the axis of the $\tau_{\text{had-vis}}$ candidate [72, 73]. These objects are further required to have a visible transverse momentum (p_{T}^{τ}) of at least 40 GeV and to be within $|\eta| < 2.3$. The output of boosted decision tree (BDT) algorithm [74] is used in order to distinguish $\tau_{\text{had-vis}}$ candidates from jets not initiated by hadronically decaying τ leptons. This is done separately for decays with one or three charged-particle tracks. In this analysis, a working point corresponding to a 55% (40%) efficiency for the identification of 1-prong (3-prong) $\tau_{\text{had-vis}}$ objects is used, with rejection rates of $O(10^2)$ for jets.

Electron candidates [75] are reconstructed from energy deposits (clusters) in the electromagnetic calorimeter, associated with a reconstructed track in the inner detector. The pseudorapidity range for the electromagnetic clusters covers the fiducial volume of the inner detector, $|\eta| < 2.47$ (the transition region between the barrel and end-cap calorimeters, $1.37 < |\eta| < 1.52$, is excluded). Quality requirements on the EM shower and the track, as well as isolation requirements, based on its transverse energy and the tracking information, are then applied in order to reduce contamination from jets. Muon candidates are reconstructed from track segments in the muon spectrometer, and matched with tracks found in the inner detector within $|\eta| < 2.5$ [76]. The final muon tracks are refitted using the complete track information from both detector systems. They must fulfil quality requirements including a p_{T}-dependent track-based isolation requirement. In this analysis, events with isolated electron or muon candidates with a transverse energy or momentum above 20 GeV are rejected.

When objects overlap geometrically, the following procedure is applied. Electrons are removed if found within ΔR of 0.2 around the axis of a muon. Then, every $\tau_{\text{had-vis}}$ candidate that overlaps with a electron or muon, within a cone of size ΔR of 0.2, is removed. Finally, reconstructed jets are discarded if an electron or a $\tau_{\text{had-vis}}$ candidate fulfilling the selection criteria above is found within a cone of size ΔR of 0.2.

The magnitude $E_{\text{T}}^{\text{miss}}$ of the missing transverse momentum [77] is reconstructed from the negative vector sum of transverse momenta of reconstructed and fully calibrated objects (collected in the hard term), as well as from reconstructed tracks associated with the hard-scatter vertex which are not in the hard term (collected in the soft term). In order to mitigate the effects of pile-up, the $E_{\text{T}}^{\text{miss}}$ is refined by using object-level corrections for the identified electrons, muons, jets and $\tau_{\text{had-vis}}$ candidates in the hard term. As the soft term contains only tracks associated with the hard-scatter vertex, it is robust against pile-up.

4 Event selection

Charged Higgs bosons are searched for in the following topology: $pp \to [b]tH^+ \to [b](jjb)(\tau_{\text{had}}\nu)$, i.e both the W boson in the top-quark decay and the τ lepton decay hadronically.

Events collected using an $E_{\text{T}}^{\text{miss}}$ trigger with a threshold at 70 (90) GeV for 2015 (2016) data are considered. After ensuring that no jets are consistent with having originated from instrumental effects or non-collision background, the following event-level requirements are made:

- One $\tau_{\text{had-vis}}$ candidate with $p_{\text{T}}^{\tau} > 40$ GeV (only the highest-p_{T}^{τ} object is considered as the τ_{had} candidate and is required to fulfil the identification criteria described in Section 3);
- Three or more jets with $p_{\text{T}} > 25$ GeV, of which at least one is b-tagged;

[5] $\Delta R = \sqrt{(\Delta\eta)^2 + (\Delta\phi)^2}$, where $\Delta\eta$ and $\Delta\phi$ are differences in pseudorapidity and azimuthal angle, respectively.

- No electron or muon with a transverse energy or momentum above 20 GeV;
- $E_{\mathrm{T}}^{\mathrm{miss}} > 150$ GeV.

The $E_{\mathrm{T}}^{\mathrm{miss}}$ trigger efficiency is measured in data and then used to reweight the simulated events, rather than relying on the modeling of $E_{\mathrm{T}}^{\mathrm{miss}}$ trigger in the simulation. This measurement is performed in a control region of the data that is orthogonal to the signal region described above, while retaining as many similarities as possible. For this purpose, events passing a single-electron trigger with a transverse energy threshold at 24 GeV are considered and required to contain exactly one electron matched to the corresponding trigger object, exactly one $\tau_{\text{had-vis}}$ and two or more jets, of which at least one is b-tagged. Both the electron and the $\tau_{\text{had-vis}}$ fulfil loose identification criteria in order to improve the statistical precision, with little impact on the measured $E_{\mathrm{T}}^{\mathrm{miss}}$ turn-on curve. The trigger efficiency measurement is performed separately for two different triggers used in 2015 and 2016.

For the selected events, the transverse mass m_{T} of the $\tau_{\text{had-vis}}$ and $E_{\mathrm{T}}^{\mathrm{miss}}$ system is used a discriminant variable for the search, is defined as:

$$m_{\mathrm{T}} = \sqrt{2 p_{\mathrm{T}}^{\tau} E_{\mathrm{T}}^{\mathrm{miss}} (1 - \cos \Delta\phi_{\tau, E_{\mathrm{T}}^{\mathrm{miss}}})}, \tag{1}$$

where $\Delta\phi_{\tau, E_{\mathrm{T}}^{\mathrm{miss}}}$ is the azimuthal angle between the $\tau_{\text{had-vis}}$ and the direction of the missing transverse momentum. In the τ+jets channel, this discriminating variable takes values lower than the W boson mass for $W \to \tau\nu$ decays in background events and lower than the H^+ mass for signal events, in the absence of detector resolution effects.

A requirement of $m_{\mathrm{T}} > 50$ GeV is applied in order to reject events with mismeasured $E_{\mathrm{T}}^{\mathrm{miss}}$, where $\tau_{\text{had-vis}}$ is nearly aligned with the direction of the missing transverse momentum.

5 Background modelling

In this search, the backgroung processes are $t\bar{t}$, single-top-quark, W+jets, Z/γ^*+jets, diboson and multi-jet (MJ) events. Backgrounds are categorised based on the object that gives rise to the identified $\tau_{\text{had-vis}}$.

The "jet $\to \tau_{\text{had-vis}}$" background includes multi-jet events and other processes where a quark- or gluon-initiated jet is reconstructed and selected as the $\tau_{\text{had-vis}}$ candidate. This background is estimated with a data-driven method. For this purpose, a control region populated primarily with misidentified $\tau_{\text{had-vis}}$ candidates is defined by using the same requirements as for the τ+jets signal region, except that $E_{\mathrm{T}}^{\mathrm{miss}} < 80$ GeV and that the number of b-tagged jets is zero. The fake factor (FF) is defined as the ratio of the number of misidentified $\tau_{\text{had-vis}}$ candidates fulfilling the nominal object selection to the number of misidentified $\tau_{\text{had-vis}}$ candidates satisfying an "anti-$\tau_{\text{had-vis}}$" selection. This anti-$\tau_{\text{had-vis}}$ selection is defined by inverting the $\tau_{\text{had-vis}}$ identification criteria while maintaining a loose requirement on the BDT output score, which selects the similar kind of objects mimicking $\tau_{\text{had-vis}}$ candidates as those fulfilling the identification criteria. The FFs are parameterised as functions of p_{T} and number of tracks in the τ_{had} decay, separately for the data collected in 2015 and 2016, as illustrated in Figure 2. After subtracting $\tau_{\text{had-vis}}$ candidates not fulfilling the

identification criteria but matching a true τ_{had} at generator level, the number of events with a misidentified $\tau_{\text{had-vis}}$ in the signal region ($N_{\text{fakes}}^{\tau_{\text{had-vis}}}$) is derived from the subset of anti-$\tau_{\text{had-vis}}$ candidates as follows:

$$N_{\text{fakes}}^{\tau_{\text{had-vis}}} = \sum_i N_{\text{anti}-\tau_{\text{had-vis}}}(i) \times \text{FF}(i), \tag{2}$$

where the index i refers to each bin in terms of p_{T} and number of tracks in the τ_{had} decay (two categories: 1-prong and 3-prong), in which the FF is evaluated. FF's derived the way described above show a limited dependence on the average number of collisions per bunch crossing (pileup). It has been checked that, due to selection bias, the profile of the pileup is not exactly identical in the signal region and the control region used for FF extraction. A corresponding systematic uncertainty has been attributed.

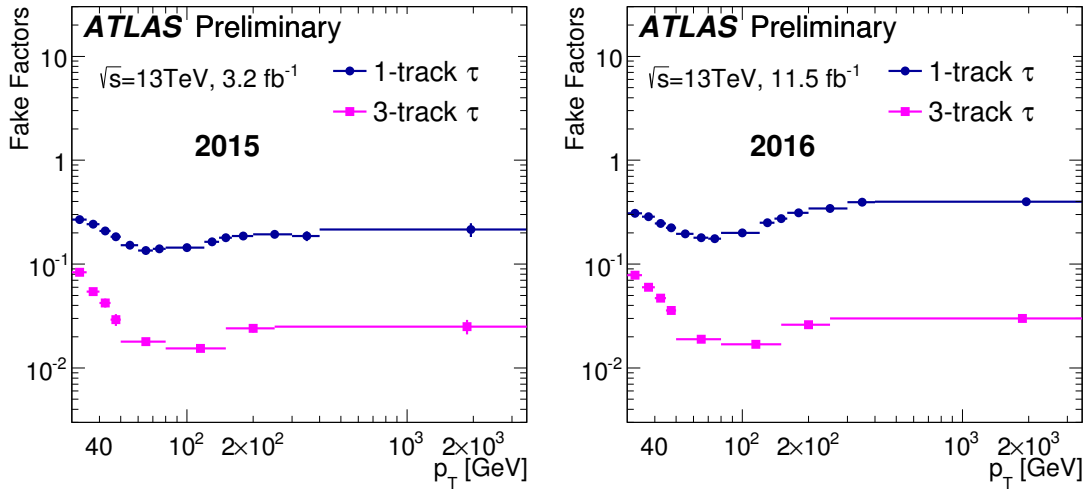

Figure 2: Fake factors parameterised as a function of p_{T}^{τ} and the number of charged decay products (two categories: 1-prong and 3-prong) as obtained for 2015 data (left) and 2016 data (right).

Backgrounds arising from events in which an isolated electron or muon is misidentified as a $\tau_{\text{had-vis}}$ only contribute at the level of 3% to the total background, with misidentified muons contributing about one order of magnitude less than misidentified electrons. These backgrounds are estimated with simulation and include contributions from $t\bar{t}$, single-top-quark, W/Z+jets and diboson processes. If an electron is misidentified as a $\tau_{\text{had-vis}}$, a correction factor is applied to the event in order to account for the misidentification rate measured in data in $Z \to e^+e^-$ on-shell events, where one electron is reconstructed as a $\tau_{\text{had-vis}}$.

The backgrounds with a true τ_{had} are estimated using simulation. The two dominant processes, $t\bar{t}$ and $W \to \tau\nu$, are validated in two dedicated control regions, which differ from the nominal event selection by the requirements that $m_{\text{T}} < 100$ GeV, and that the number of b-tagged jets be either at least two (for the control region enriched with $t\bar{t}$ events) or zero (for the control region enriched with $W \to \tau\nu$ events). The m_{T} distributions that are predicted and measured in the above background-enriched control regions are displayed in Figures 3 and 4. The relative signal contamination in the control region enriched in $W \to \tau\nu$ events is about two orders of magnitude smaller than the expected fraction of $H^+ \to \tau\nu$ events in the signal region. The control region enriched in $t\bar{t}$ events has a small overlap with the signal region, as

the expected signal contamination is about one order of magnitude smaller than the expected fraction of $H^+ \to \tau\nu$ events in the signal region.

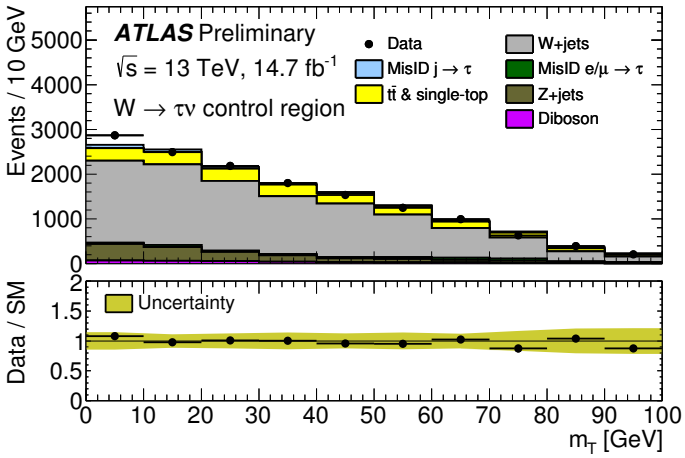

Figure 3: Distribution of m_{T} in the τ+jets validation region enriched with $W \to \tau\nu$ events, which differs from the nominal event selection by the requirements that $m_{\mathrm{T}} < 100$ GeV and that the number of b-tagged jets be zero. The $W \to \tau\nu$ background is normalised to the data through an overall scale factor. The total (statistical and systematic) uncertainties in the SM prediction are shown in the lower plot.

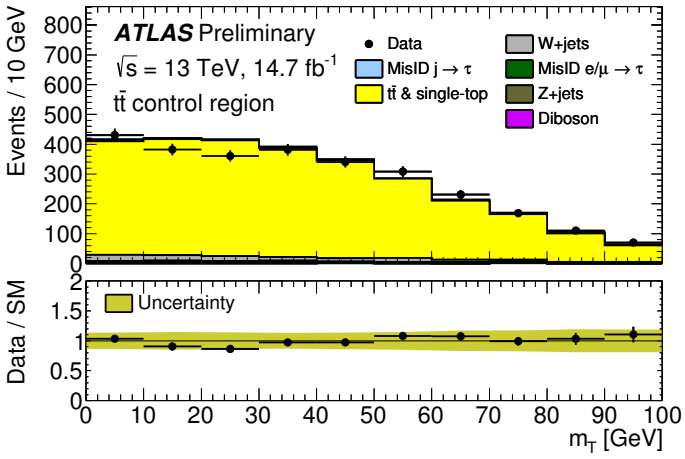

Figure 4: Distribution of m_{T} in the τ+jets validation region enriched with $t\bar{t}$ events, which differs from the nominal event selection by the requirements that $m_{\mathrm{T}} < 100$ GeV and that the number of b-tagged jets be at least two. The total (statistical and systematic) uncertainties in the SM prediction are shown in the lower plot.

The expected number of background events in the signal region is shown in Table 1, together with the contribution expected from a hypothetical charged Higgs boson with a mass of 200 or 1000 GeV, and with $\sigma(pp \to [b]tH^+) \times \mathrm{BR}(H^+ \to \tau\nu)$ set to the prediction from the hMSSM scenario for $\tan\beta = 60$ (for a given mass, the expected signal yield increases quadratically with $\tan\beta$). The calculation of the production cross section is based on Refs. [9, 36, 78–80], while HDECAY [81, 82] is used for computing

the branching fraction. The signal acceptance at 200 (1000) GeV is 1.1% (10%), as evaluated with respect to simulated samples where both the τ-lepton and the associated top quark decay inclusively. The event yield observed in 14.7 fb^{-1} of data is also shown in Table 1 and found to be consistent with the expectation for the background-only hypothesis.

Sample	Event yield
True τ_{had}	
$t\bar{t}$ & single-top-quark	2880 ± 770 ± 25
$W \to \tau\nu$	265 ± 51 ± 18
$Z \to \tau\tau$	43 ± 6.8 ± 7.6
diboson (WW, WZ, ZZ)	13.8 ± 2.2 ± 1.7
Misidentified e, $\mu \to \tau_{\text{had-vis}}$	126 ± 24 ± 6.5
Misidentified jet $\to \tau_{\text{had-vis}}$	1170 ± 110 ± 16
All backgrounds	4500 ± 800 ± 36
H^+ (200 GeV), hMSSM tan $\beta = 60$	523 ± 86 ± 4
H^+ (1000 GeV), hMSSM tan $\beta = 60$	7.5 ± 0.6 ± 0.05
Data	4645

Table 1: Expected event yields for the backgrounds and a hypothetical H^+ signal after all selection criteria, and comparison with 14.7 fb^{-1} of data. The values shown for the signal assume a charged Higgs boson mass of 200 or 1000 GeV, with a cross section times branching fraction $\sigma(pp \to [b]tH^{\pm}) \times \text{BR}(H^{\pm} \to \tau\nu)$ corresponding to tan $\beta = 60$ in the hMSSM benchmark scenario. The sytematic and statistical uncertainties are given, respectively. Sources of systematic uncertainty are correlated amongst backgrounds when evaluating the uncertainty on the total background.

6 Systematic uncertainties

Several sources of systematic uncertainty, affecting the normalisation of signal and background processes or the shape of their transverse mass distributions, are considered. The individual sources of systematic uncertainty are assumed to be uncorrelated. However, when applied to different Monte Carlo samples, correlations of a given systematic uncertainty are treated as correlated across the processes. All systematic uncertainties are symmetrised with respect to the nominal value.

All instrumental systematic uncertainties arising from the reconstruction, identification and energy scale of electrons, muons, (b-tagged) jets and $\tau_{\text{had-vis}}$ candidates are considered, including their impact on the reconstructed $E_{\text{T}}^{\text{miss}}$. The dominant detector-related systematic uncertainties for this search arise from the jet energy scale, from the reconstruction and identification of $\tau_{\text{had-vis}}$ candidates, from the $\tau_{\text{had-vis}}$ energy scale and from the b-tagging efficiency. Their impacts on the predicted event yield for the dominant background process ($t\bar{t}$) are, 11.0%, +5.7/-3.3%, 3.6% and 1.4%. Systematic uncertainties arising from the reconstruction, identification and energy scale of electrons and muons are very small in this analysis. The luminosity uncertainties of 2.1% (3.7%) for data collected in 2015 (2016) is applied directly to the event yields of all simulated events.

The efficiency of the $E_{\text{T}}^{\text{miss}}$ trigger is measured in a control region of the data, as described in Section 4. The parameterisation of the efficiency shows a small dependence on the identification criteria (loose versus nominal) for the electron and the $\tau_{\text{had-vis}}$ candidate, as well as on the minimum number of jets chosen for

the control region. This results in small variations of the measured fit function. These variations, as well as the limited statistical precision of the bins used for the fit function and the resulting parameterisation, are accounted for as systematic uncertainties. In the signal region, the total systematic uncertainty arising from the $E_{\mathrm{T}}^{\mathrm{miss}}$ trigger efficiency measurement is about 2%.

In the estimation of backgrounds with jets misidentified as $\tau_{\text{had-vis}}$, the dominant systematic uncertainties arise from the requirement on the BDT score in the anti-$\tau_{\text{had-vis}}$ control sample, from the level of contamination of $\tau_{\text{had-vis}}$ objects matching a true τ_{had} decay at generator level and fulfilling the anti-$\tau_{\text{had-vis}}$ selection (varied by 50%) and from the statistical limitation due to the control sample size. When changing the BDT score cut, different fractions of gluon- and quark-initiated jets populate the anti-$\tau_{\text{had-vis}}$ control region. The event topology (in particular the shape of the $E_{\mathrm{T}}^{\mathrm{miss}}$ and $\Delta\phi_{\tau,\mathrm{miss}}$ distributions) also depends on the requirement imposed on the BDT score. The corresponding systematic uncertainty is assessed by considering the shape of the m_{T} distribution obtained for two alternative cuts on the BDT score, which are symmetric around the nominal cut value. The impacts of the three systematic uncertainties listed above on the event yield of the background with jets misidentified as $\tau_{\text{had-vis}}$ are, respectively, up to 20%, 6% and 3%.

The dominant background process with a true τ_{had} is the production of $t\bar{t}$ pairs and single-top-quark events, for which an overall cross-section uncertainty of 6% is applied, incorporating scale, PDF+α_{s} and top-quark mass uncertainties [51, 83, 84]. In addition, systematic uncertainties due to the choice of parton shower and hadronisation models are derived by comparing $t\bar{t}$ events generated with Powheg-Box interfaced to either Pythia v6.4 or Herwig++ v2.7.1 [85], which uses the UEEE5 [86] underlying-event tune. The systematic uncertainties arising from initial- and final-state parton radiation, which modify the jet production rate, are computed with the same packages as for the baseline $t\bar{t}$ event generation, by setting the corresponding parameters in Pythia to a range of values not excluded by the experimental data. Finally, the uncertainty due to the choice of matrix-element generator is evaluated by comparing samples generated with MadGraph5_aMC@NLO or Powheg-Box, both using the CT10 PDF set and interfaced to Herwig++ with CTEQ6L1 and UEEE5 tune. The impacts of the three systematic uncertainties listed above on the event yield of the $t\bar{t}$ background are, respectively, 16%, 7% and 15%.

For the sub-leading background process with a true τ_{had}, $W \to \tau\nu$, a systematic uncertainty of 5% is assigned to the overall renormalisation factor, as obtained by changing various selection criteria for the control region enriched with such background events. For Z+jets and diboson production, theoretical uncertainties of 5% and 6% are considered, respectively, combining PDF+α_{s} and scale variation uncertainties in quadrature.

Systematic uncertainties in the H^+ signal generation are estimated as follows. The uncertainty arising from the QCD scale is obtained by varying the factorisation and renormalisation scale up and down by a factor of two. The largest variation of the signal acceptance is then symmetrised and taken as the scale uncertainty, 4–8% depending on the mass hypothesis. The variation of the signal acceptance with various PDF sets is estimated using LHAPDF [87], but is found to be negligible for all signal samples. Finally, the impact of A14 tune variations on the signal acceptance is estimated by adding in quadrature the excursions from a subset of tune variations that cover underlying-event and jet-structure effects, as well as different aspects of extra jet production. This uncertainty amounts to 8–10%.

7 Results

In order to test the compatibility of the data with the background-only and signal+background hypotheses, a profile likelihood ratio [88] is used, with m_{T} as the discriminating variable. The statistical analysis is based on a binned likelihood function for the m_{T} distribution. All systematic uncertainties from theoretical or experimental sources are implemented as nuisance parameters. The parameter of interest $\mu \equiv \sigma(pp \to [b]tH^+) \times \mathrm{BR}(H^+ \to \tau\nu)$, and the nuisance parameters are simultaneously fitted by means of a negative log-likelihood minimisation. Expected limits are derived using the asymptotic approximation of the distribution of the test statistic [89].

Figure 5 shows the m_{T} distribution obtained after a fit with the background-only hypothesis, together with the m_{T} distributions corresponding to two H^+ mass hypotheses: 200 and 1000 GeV. The binning shown in Figure 5 is also used in the statistical analysis. The SM predictions are found to be consistent with the data, and exclusion limits are set on $\sigma(pp \to [b]tH^+) \times \mathrm{BR}(H^+ \to \tau\nu)$ at the 95% confidence level (CL) using the CL_s procedure [90]. Figure 6 shows the observed and expected exclusion limits as a function of H^+ mass hypothesis. They agree within the uncertainties over the explored H^+ mass range. The observed limits range from 2.0 to 0.008 pb in the mass range 200–2000 GeV. The impact from the various sources of systematic uncertainty on the expected 95% CL exclusion limits are summarised in Table 2, for H^+ mass hypotheses of 200 and 1000 GeV. The impact is obtained by comparing the nominal expected limit with the expected limit when a certain set of uncertainties is not included in the limit-setting procedure. The impact of the systematic uncertainties reported in Section 6 only represents the relative change in event yields. In the limit-setting procedure, however, m_{T} shape variations are also taken into account, leading to a different relative importance of the various systematic uncertainties. The systematic uncertainties with a large impact over the explored mass range are the $\tau_{\text{had-vis}}$ identification and energy-scale uncertainties, the $t\bar{t}$ background modelling uncertainties, and the estimation of the background with a jet misidentified as a $\tau_{\text{had-vis}}$. The total uncertainty is dominated by the statistical uncertainty.

The limits in Figure 6 are presented together with an illustrative signal prediction in the hMSSM benchmark scenario. Figure 7 shows the 95% CL exclusion limits on $\tan\beta$ as a function of m_{H^+} in the context of the hMSSM scenario, compared with the 2015 results reported in Ref. [21]. Values of $\tan\beta$ in the range 42–60 are excluded for a charged Higgs boson mass of 200 GeV. At $\tan\beta = 60$, above which no reliable theoretical calculations exist, the H^+ mass range from 200 to 540 GeV is excluded. As a result of the new choice of QCD scale for the H^+ signal generation, the expected limit at 200 GeV is not improved relative to the one obtained in 2015 [21]. However, at high mass, the limit is largely improved.

8 Conclusion

A search for charged Higgs bosons produced in association with a single top quark and subsequently decaying via $H^+ \to \tau\nu$ is performed, based on fully hadronic final states. The dataset used for this analysis contains 14.7 fb^{-1} of pp collisions at $\sqrt{s} = 13$ TeV, recorded in 2015 and 2016 by the ATLAS detector at the LHC. The background-only hypothesis is found to be in agreement with the data. Upper limits are set on the production cross section times branching fraction between 2.0 and 0.008 pb for a charged Higgs boson mass range of 200–2000 GeV. In the context of the hMSSM, values of $\tan\beta$ in the range 42–60 are excluded for a charged Higgs boson mass of 200 GeV. The H^+ mass range from 200 to 540 GeV is excluded at $\tan\beta = 60$.

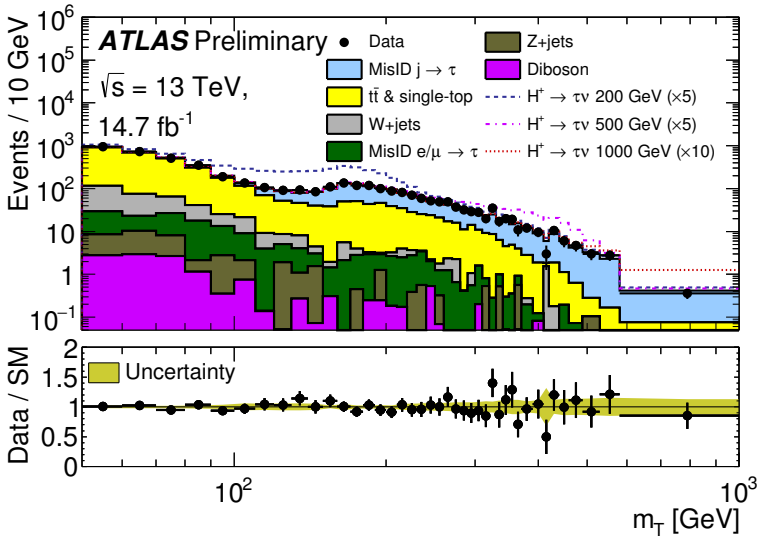

Figure 5: Distribution of m_{T} after full event selection and a fit to the data with the background-only hypothesis. The horizontal axis starts at $m_{\mathrm{T}} = 50$ GeV and is in logarithmic scale. Three H^+ signal hypotheses are included separately on the stack. The signal samples at 200, 500 and 1000 GeV are scaled, respectively, to 5, 5 and 10 times the cross section predicted at $\tan\beta = 60$ in the hMSSM benchmark scenario. Bins have a varying size. The last bin includes all overflow events. The total (statistical and systematic) uncertainties in the SM prediction, as obtained from the binned profile likelihood ratio fit, are shown in the lower plot.

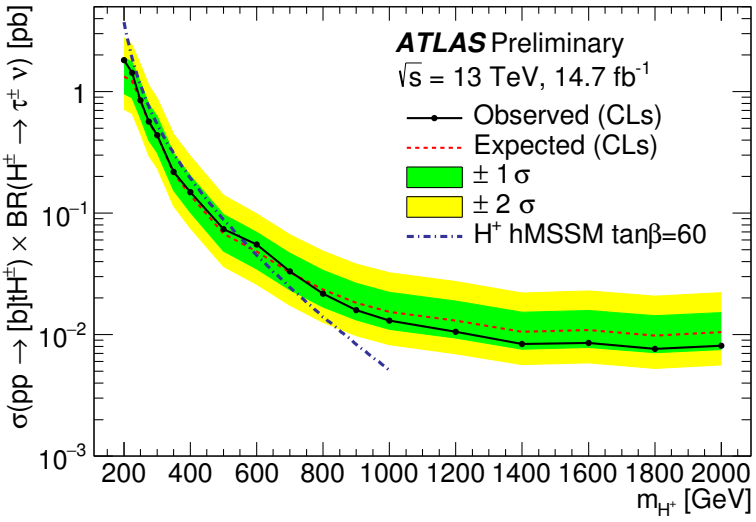

Figure 6: Observed and expected 95% CL exclusion limits for heavy charged Higgs boson production as a function of m_{H^+} in 14.7 fb^{-1} of pp collision data at $\sqrt{s} = 13$ TeV. The prediction for $\sigma(pp \to [b]tH^+) \times \mathrm{BR}(H^+ \to \tau\nu)$ as a function of the charged Higgs boson mass is also shown as a dotted-dashed line, for $\tan\beta = 60$ in the hMSSM benchmark scenario.

Source of systematic uncertainty	Impact on the expected limit (in %) m_{H^+} = 200 GeV	m_{H^+} = 1000 GeV
Experimental		
luminosity	1.5	0.9
trigger	< 0.1	< 0.1
$\tau_{\text{had-vis}}$	1.0	1.4
jet	3.0	0.2
$E_{\text{T}}^{\text{miss}}$	< 0.1	< 0.1
Fake factors	0.8	4.7
Signal and background models		
$t\bar{t}$ modelling	13.2	3.5
H^+ signal modelling	1.4	1.4

Table 2: Impact of various sources of uncertainty on the expected 95% CL exclusion limit, for two H^+ mass hypotheses: 200 and 1000 GeV. The impact is obtained by comparing the nominal expected limit with the expected limit when a certain set of uncertainties is not included in the limit-setting procedure.

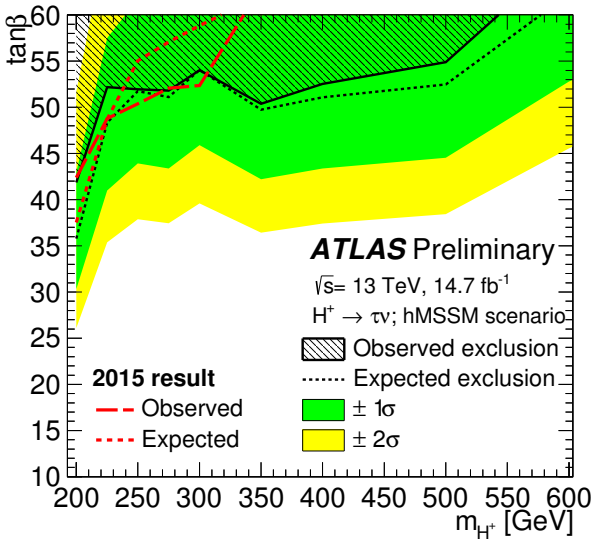

Figure 7: 95% CL exclusion limits on $\tan\beta$ as a function of m_{H^+}, shown in the context of the hMSSM, for the regions in which reliable theoretical calculations exist ($\tan\beta \leq 60$). As a comparison, the red curves show the observed and expected exclusion limits measured at $\sqrt{s} = 13$ TeV in 2015 by ATLAS [21].

References

[1] ATLAS Collaboration, *Observation of a new particle in the search for the Standard Model Higgs boson with the ATLAS detector at the LHC*, Phys. Lett. B **716** (2012) 1, arXiv: 1207.7214 [hep-ex].

[2] CMS Collaboration, *Observation of a new boson at a mass of 125 GeV with the CMS experiment at the LHC*, Phys. Lett. B **716** (2012) 30, arXiv: 1207.7235 [hep-ex].

[3] T. D. Lee, *A Theory of Spontaneous T Violation*, Phys. Rev. D **8** (1973) 1226.

[4] T. P. Cheng and L.-F. Li,
Neutrino Masses, Mixings and Oscillations in SU(2)×U(1) Models of Electroweak Interactions,
Phys. Rev. D **22** (1980) 2860.

[5] J. Schechter and J. W. F. Valle, *Neutrino Masses in SU(2)×U(1) Theories*,
Phys. Rev. D **22** (1980) 2227.

[6] G. Lazarides, Q. Shafi and C. Wetterich,
Proton Lifetime and Fermion Masses in an SO(10) Model, Nucl. Phys. B **181** (1981) 287.

[7] R. N. Mohapatra and G. Senjanovic,
Neutrino Masses and Mixings in Gauge Models with Spontaneous Parity Violation,
Phys. Rev. D **23** (1981) 165.

[8] M. Magg and C. Wetterich, *Neutrino Mass Problem and Gauge Hierarchy*,
Phys. Lett. B **94** (1980) 61.

[9] J. R. Andersen et al., *Handbook of LHC Higgs Cross Sections: 3. Higgs Properties*,
CERN-2013-004 (2013), arXiv: 1307.1347 [hep-ph].

[10] M. Carena et al., *MSSM Higgs Boson Searches at the LHC: Benchmark Scenarios after the Discovery of a Higgs-like Particle*, Eur. Phys. J. C **73** (2013) 2552, arXiv: 1302.7033 [hep-ph].

[11] A. Djouadi et al., *The post-Higgs MSSM scenario: Habemus MSSM?*,
Eur. Phys. J. C **73** (2013) 2650, arXiv: 1307.5205 [hep-ph].

[12] E. Bagnaschi et al., *Benchmark scenarios for low* $\tan\beta$ *in the MSSM*, LHCHXSWG-2015-002,
URL: http://cdsweb.cern.ch/record/2039911.

[13] ATLAS Collaboration, *Search for charged Higgs bosons decaying via* $H^+ \to \tau\nu$ *in top quark pair events using pp collision data at* $\sqrt{s} = 7$ *TeV with the ATLAS detector*, JHEP **06** (2012) 039,
arXiv: 1204.2760 [hep-ex].

[14] ATLAS Collaboration, *Search for charged Higgs bosons through the violation of lepton universality in* $t\bar{t}$ *events using pp collision data at* $\sqrt{s} = 7$ *TeV with the ATLAS experiment*,
JHEP **03** (2013) 076, arXiv: 1212.3572 [hep-ex].

[15] ATLAS Collaboration, *Search for charged Higgs bosons decaying via* $H^+ \to \tau\nu$ *in fully hadronic final states using pp collision data at* $\sqrt{s} = 8$ *TeV with the ATLAS detector*, JHEP **03** (2015) 088,
arXiv: 1412.6663 [hep-ex].

[16] CMS Collaboration,
Search for a light charged Higgs boson in top quark decays in pp collisions at $\sqrt{s} = 7$ *TeV*,
JHEP **07** (2012) 143, arXiv: 1205.5736 [hep-ex].

[17] CMS Collaboration, *Search for a charged Higgs boson in pp collisions at* $\sqrt{s} = 8$ *TeV*,
JHEP **11** (2015) 018, arXiv: 1508.07774 [hep-ex].

[18] ATLAS Collaboration, *Search for a light charged Higgs boson in the decay channel* $H^+ \to c\bar{s}$ *in* $t\bar{t}$ *events using pp collisions at* $\sqrt{s} = 7$ *TeV with the ATLAS detector*,
Eur. Phys. J. C **73** (2013) 2465, arXiv: 1302.3694 [hep-ex].

[19] CMS Collaboration,
Search for a light charged Higgs boson decaying to $c\bar{s}$ *in pp collisions at* $\sqrt{s} = 8$ *TeV*,
JHEP **12** (2015) 178, arXiv: 1510.04252 [hep-ex].

[20] ATLAS Collaboration, *Search for charged Higgs bosons in the $H^{\pm} \to tb$ decay channel in pp collisions at $\sqrt{s} = 8$ TeV using the ATLAS detector*, JHEP **03** (2016) 127, arXiv: 1512.03704 [hep-ex].

[21] ATLAS Collaboration, *Search for charged Higgs bosons produced in association with a top quark and decaying via $H^{\pm} \to \tau\nu$ using pp collision data recorded at $\sqrt{s} = 13$ TeV by the ATLAS detector*, Phys. Lett. B **759** (2016) 555, arXiv: 1603.09203 [hep-ex].

[22] ATLAS Collaboration, *Search for a Charged Higgs Boson Produced in the Vector-boson Fusion Mode with Decay $H^{+} \to WZ$ using pp Collisions at $\sqrt{s} = 8$ TeV with the ATLAS Experiment*, Phys. Rev. Lett. **114** (2015) 231801, arXiv: 1503.04233 [hep-ex].

[23] ATLAS Collaboration, *Search for charged Higgs bosons in the $H^{\pm} \to tb$ decay channel in pp collisions at $\sqrt{s}$=13 TeV using the ATLAS detector*, ATLAS-CONF-2016-089, URL: https://atlas.web.cern.ch/Atlas/GROUPS/PHYSICS/CONFNOTES/ATLAS-CONF-2016-089/.

[24] R. M. Barnett, H. E. Haber and D. E. Soper, *Ultra-heavy particle production from heavy partons at hadron colliders*, Nucl. Phys. B **306** (1988) 697.

[25] A. C. Bawa, C. S. Kim and A. D. Martin, *Charged Higgs production at hadron colliders*, Z. Phys. C **47** (1990) 75.

[26] V. D. Barger, R. J. N. Phillips and D. P. Roy, *Heavy charged Higgs signals at the LHC*, Phys. Lett. B **324** (1994) 236, arXiv: hep-ph/9311372.

[27] R. Harlander, M. Krämer and M. Schumacher, *Bottom-quark associated Higgs-boson production: reconciling the four- and five-flavour scheme approach*, (2011), arXiv: 1112.3478 [hep-ph].

[28] ATLAS Collaboration, *The ATLAS experiment at the CERN Large Hadron Collider*, JINST **3** (2008) S08003.

[29] ATLAS Collaboration, *Early inner detector tracking performance in the 2015 data at $\sqrt{s} = 13$ TeV*, ATL-PHYS-PUB-2015-051, URL: http://cdsweb.cern.ch/record/2110140.

[30] ATLAS Collaboration, *2015 start-up trigger menu and initial performance assessment of the ATLAS trigger using Run-2 data*, ATL-DAQ-PUB-2016-001, URL: http://cdsweb.cern.ch/record/2136007.

[31] ATLAS Collaboration, *Improved luminosity determination in pp collisions at $\sqrt{s} = 7$ TeV using the ATLAS detector at the LHC*, Eur. Phys. J. C **73** (2013) 2518, arXiv: 1302.4393 [hep-ex].

[32] J. Alwall et al., *The automated computation of tree-level and next-to-leading order differential cross sections, and their matching to parton shower simulations*, JHEP **07** (2014) 158, arXiv: 1405.0301 [hep-ph].

[33] R. D. Ball et al., *Parton distributions with LHC data*, Nucl. Phys. B **867** (2013) 244, arXiv: 1207.1303 [hep-ph].

[34] T. Sjöstrand, S. Mrenna and P. Z. Skands, *A Brief Introduction to PYTHIA 8.1*, Comput. Phys. Commun. **178** (2008) 852, arXiv: 0710.3820 [hep-ph].

[35] ATLAS Collaboration, *ATLAS Pythia 8 tunes to 7 TeV data*, ATL-PHYS-PUB-2014-021, URL: http://cdsweb.cern.ch/record/1966419.

[36] C. Degrande et al., *Heavy charged Higgs boson production at the LHC*, JHEP **10** (2015) 145, arXiv: 1507.02549 [hep-ph].

[37] S. Frixione, P. Nason and G. Ridolfi, *A Positive-Weight Next-to-Leading-Order Monte Carlo for Heavy Flavour Hadroproduction*, JHEP **09** (2007) 126, arXiv: 0707.3088 [hep-ph].

[38] S. Alioli et al., *A general framework for implementing NLO calculations in shower Monte Carlo programs: the POWHEG BOX*, JHEP **06** (2010) 043, arXiv: 1002.2581 [hep-ph].

[39] H.-L. Lai et al., *New parton distributions for collider physics*, Phys. Rev. D **82** (2010) 074024, arXiv: 1007.2241 [hep-ph].

[40] J. Gao et al., *The CT10 NNLO global analysis of QCD*, Phys.Rev. D **89** (2014) 033009, arXiv: 1302.6246 [hep-ph].

[41] P. Artoisenet et al., *Automatic spin-entangled decays of heavy resonances in Monte Carlo simulations*, JHEP **03** (2013) 015, arXiv: 1212.3460 [hep-ph].

[42] T. Sjöstrand et al., *High-energy physics event generation with PYTHIA 6.1*, Comput. Phys. Commun. **135** (2001) 238, arXiv: hep-ph/0010017.

[43] P. M. Nadolsky et al., *Implications of CTEQ global analysis for collider observables*, Phys. Rev. D **78** (2008) 013004, arXiv: 0802.0007 [hep-ph].

[44] P. Z. Skands, *Tuning Monte Carlo Generators: The Perugia Tunes*, Phys. Rev. D **82** (2010) 074018, arXiv: 1005.3457 [hep-ph].

[45] M. Cacciari et al., *Top-pair production at hadron colliders with next-to-next-to-leading logarithmic soft-gluon resummation*, Phys. Lett. B **710** (2012) 612, arXiv: 1111.5869 [hep-ph].

[46] M. Beneke et al., *Hadronic top-quark pair production with NNLL threshold resummation*, Nucl. Phys. B **855** (2012) 695, arXiv: 1109.1536 [hep-ph].

[47] P. Bärnreuther, M. Czakon and A. Mitov, *Percent Level Precision Physics at the Tevatron: First Genuine NNLO QCD Corrections to $q\bar{q} \to t\bar{t} + X$*, Phys. Rev. Lett. **109** (2012) 132001, arXiv: 1204.5201 [hep-ph].

[48] M. Czakon and A. Mitov, *NNLO corrections to top-pair production at hadron colliders: the all-fermionic scattering channels*, JHEP **12** (2012) 054, arXiv: 1207.0236 [hep-ph].

[49] M. Czakon and A. Mitov, *NNLO corrections to top pair production at hadron colliders: the quark-gluon reaction*, JHEP **01** (2013) 080, arXiv: 1210.6832 [hep-ph].

[50] M. Czakon, P. Fiedler and A. Mitov, *Total Top-Quark Pair-Production Cross Section at Hadron Colliders Through $O(\alpha_S^4)$*, Phys. Rev. Lett. **110** (2013) 252004, arXiv: 1303.6254 [hep-ph].

[51] M. Czakon and A. Mitov, *Top++: A Program for the Calculation of the Top-Pair Cross-Section at Hadron Colliders*, Comput. Phys. Commun. **185** (2014) 2930, arXiv: 1112.5675 [hep-ph].

[52] N. Kidonakis, *Next-to-next-to-leading-order collinear and soft gluon corrections for t-channel single top quark production*, Phys. Rev. D **83** (2011) 091503, arXiv: 1103.2792 [hep-ph].

[53] N. Kidonakis, *NNLL resummation for s-channel single top quark production*, Phys. Rev. D **81** (2010) 054028, arXiv: 1001.5034 [hep-ph].

[54] N. Kidonakis,
Two-loop soft anomalous dimensions for single top quark associated production with a W^- or H^-,
Phys. Rev. D **82** (2010) 054018, arXiv: 1005.4451 [hep-ph].

[55] N. Davidson, T. Przedzinski and Z. Was,
PHOTOS Interface in C++: Technical and Physics Documentation,
Comput. Phys. Commun. **199** (2016) 86, arXiv: 1011.0937 [hep-ph].

[56] C. Anastasiou et al., *High-precision QCD at hadron colliders: electroweak gauge boson rapidity distributions at NNLO*, Phys. Rev. D **69** (2004) 094008, arXiv: hep-ph/0312266.

[57] K. Melnikov and F. Petriello,
*Electroweak gauge boson production at hadron colliders through O(alpha(s)**2)*,
Phys. Rev. D **74** (2006) 114017, arXiv: hep-ph/0609070.

[58] R. Gavin et al., *FEWZ 2.0: A code for hadronic Z production at next-to-next-to-leading order*,
Comput. Phys. Commun. **181** (2011) 2388, arXiv: 1011.3540 [hep-ph].

[59] ATLAS Collaboration, *Measurement of the Z/γ^* boson transverse momentum distribution in pp collisions at $\sqrt{s} = 7$ TeV with the ATLAS detector*, JHEP **09** (2014) 55,
arXiv: 1406.3660 [hep-ex].

[60] D. J. Lange, *The EvtGen particle decay simulation package*,
Nucl. Instrum. Meth. A **462** (2001) 152.

[61] A. D. Martin et al., *Parton distributions for the LHC*, Eur. Phys. J. C **63** (2009) 189,
arXiv: 0901.0002 [hep-ph].

[62] A. D. Martin et al., *Uncertainties on α_S in global PDF analyses and implications for predicted hadronic cross sections*, Eur. Phys. J. C **64** (2009) 653, arXiv: 0905.3531 [hep-ph].

[63] A. D. Martin et al.,
Heavy-quark mass dependence in global PDF analyses and 3- and 4-flavour parton distributions,
Eur. Phys. J. C **70** (2010) 51, arXiv: 1007.2624 [hep-ph].

[64] ATLAS Collaboration, *Summary of ATLAS Pythia 8 tunes*, ATL-PHYS-PUB-2012-003,
URL: http://cdsweb.cern.ch/record/1474107.

[65] ATLAS Collaboration, *The ATLAS Simulation Infrastructure*, Eur. Phys. J. C **70** (2010) 823,
arXiv: 1005.4568 [physics.ins-det].

[66] S. Agostinelli et al., *GEANT4 - A Simulation Toolkit*, Nucl. Instr. and Meth. A **506** (2003) 250.

[67] M. Cacciari, G. P. Salam and G. Soyez, *The anti-k_t jet clustering algorithm*, JHEP **04** (2008) 063,
arXiv: 0802.1189 [hep-ph].

[68] ATLAS Collaboration, *Tagging and suppression of pileup jets with the ATLAS detector*,
ATLAS-CONF-2014-018, URL: http://cdsweb.cern.ch/record/1700870.

[69] ATLAS Collaboration, *Expected performance of the ATLAS b-tagging algorithms in Run-2*,
ATL-PHYS-PUB-2015-022, URL: http://cdsweb.cern.ch/record/2037697.

[70] ATLAS Collaboration, *Performance of b-Jet Identification in the ATLAS Experiment*,
JINST **11** (2016) P04008, arXiv: 1512.01094 [hep-ex].

[71] ATLAS Collaboration,
Commissioning of the ATLAS b-tagging algorithms using $t\bar{t}$ events in early Run-2 data,
ATL-PHYS-PUB-2015-039, URL: http://cdsweb.cern.ch/record/2047871.

[72] ATLAS Collaboration, *Reconstruction, Energy Calibration, and Identification of Hadronically Decaying Tau Leptons in the ATLAS Experiment for Run-2 of the LHC*, ATL-PHYS-PUB-2015-045, URL: http://cdsweb.cern.ch/record/2064383.

[73] ATLAS Collaboration, *Reconstruction of hadronic decay products of tau leptons with the ATLAS experiment*, Eur. Phys. J. **C76** (2016) 295, arXiv: 1512.05955 [hep-ex].

[74] A. Höcker et al., *TMVA - Toolkit for Multivariate Data Analysis*, PoS **ACAT** (2007) 040, arXiv: physics/0703039, URL: http://pos.sissa.it/archive/conferences/050/040/ACAT_040.pdf.

[75] ATLAS Collaboration, *Electron efficiency measurements with the ATLAS detector using the 2015 LHC proton-proton collision data*, ATLAS-CONF-2016-024, URL: http://cdsweb.cern.ch/record/2157687.

[76] ATLAS Collaboration, *Muon reconstruction performance of the ATLAS detector in proton proton collision data at $\sqrt{s}$ =13 TeV*, Eur. Phys. J. **C76** (2016) 292, arXiv: 1603.05598 [hep-ex].

[77] ATLAS Collaboration, *Performance of missing transverse momentum reconstruction for the ATLAS detector in the first proton-proton collisions at $\sqrt{s}$ = 13 TeV*, ATL-PHYS-PUB-2015-027, URL: http://cdsweb.cern.ch/record/2037904.

[78] M. Flechl et al., *Improved cross-section predictions for heavy charged Higgs boson production at the LHC*, Phys. Rev. D **91** (2015) 075015, arXiv: 1409.5615 [hep-ph].

[79] S. Dittmaier et al., *Charged-Higgs-boson production at the LHC: NLO supersymmetric QCD corrections*, Phys. Rev. D **83** (2011) 055005, arXiv: 0906.2648 [hep-ph].

[80] E. L. Berger et al., *Associated production of a top quark and a charged Higgs boson*, Phys. Rev. D **71** (2005) 115012, arXiv: hep-ph/0312286 [hep-ph].

[81] A. Djouadi, J. Kalinowski and M. Spira, *HDECAY: A Program for Higgs boson decays in the standard model and its supersymmetric extension*, Comput. Phys. Commun. **108** (1998) 56, arXiv: hep-ph/9704448 [hep-ph].

[82] E. Bagnaschi et al., *Higgs production via gluon fusion in the POWHEG approach in the SM and in the MSSM*, JHEP **02** (2012) 088, arXiv: 1111.2854 [hep-ph].

[83] M. Aliev et al., *HATHOR: HAdronic Top and Heavy quarks crOss section calculatoR*, Comput. Phys. Commun. **182** (2011) 1034, arXiv: 1007.1327 [hep-ph].

[84] P. Kant et al., *HatHor for single top-quark production: Updated predictions and uncertainty estimates for single top-quark production in hadronic collisions*, Comput. Phys. Commun. **191** (2015) 74, arXiv: 1406.4403 [hep-ph].

[85] M. Bähr et al., *Herwig++ Physics and Manual*, Eur. Phys. J. C **58** (2008) 639, arXiv: 0803.0883 [hep-ph].

[86] M. H. Seymour and A. Siodmok, *Constraining MPI models using σ_{eff} and recent Tevatron and LHC Underlying Event data*, JHEP **10** (2013) 113, arXiv: 1307.5015 [hep-ph].

[87] A. Buckley et al., *LHAPDF6: parton density access in the LHC precision era*, Eur. Phys. J. C **75** (2015) 132, arXiv: 1412.7420 [hep-ph].

[88] ATLAS Collaboration, *Combined search for the Standard Model Higgs boson in pp collisions at $\sqrt{s}$=7 TeV with the ATLAS detector*, Phys. Rev. D **86** (2012) 032003, arXiv: 1207.0319 [hep-ex].

[89] G. Cowan et al., *Asymptotic formulae for likelihood-based tests of new physics*, Eur. Phys. J. C **71** (2011) 1554, [Erratum: Eur. Phys. J.C73,2501(2013)], arXiv: 1007.1727 [physics.data-an].

[90] A. L. Read, *Presentation of search results: the CL_s technique*, J. Phys. G **28** (2002) 2693.

Appendix

Figure 8 shows the 95% CL exclusion limits on $\tan\beta$ as a function of m_{H^+} in the context of the $m_h^{\text{mod}-}$ scenario, compared with the 2015 results reported in Ref. [21]. Values of $\tan\beta$ in the range 43–60 are excluded for a charged Higgs boson mass of 200 GeV. At $\tan\beta = 60$, above which no reliable theoretical calculations exist, the H^+ mass range from 200 to 530 GeV is excluded.

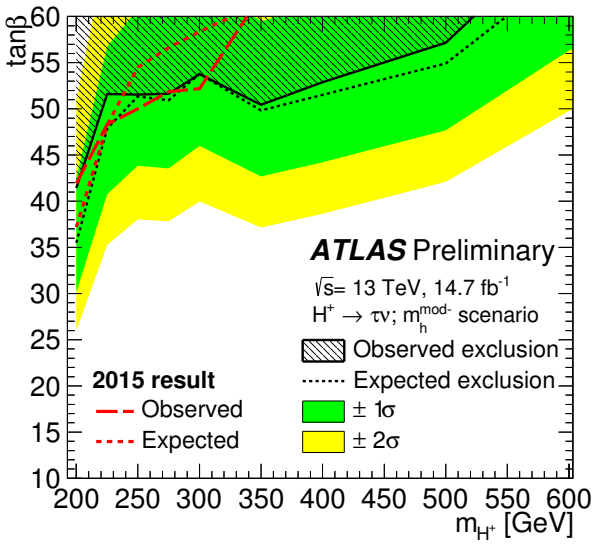

Figure 8: 95% CL exclusion limits on $\tan\beta$ as a function of m_{H^+}, shown in the context of the $m_h^{\text{mod}-}$, for the regions in which reliable theoretical calculations exist ($\tan\beta \leq 60$). As a comparison, the red curves show the observed and expected exclusion limits measured at $\sqrt{s} = 13$ TeV in 2015 by ATLAS [21].

The 2015+2016 expected limit can be compared to the one with 2015 data [21]. The comparison is shown in Figure 9. An improved sensitivity is observed over the full mass range, increasing with the mass hypothesis and reaching a factor of two at high masses ($m_{H^+} > 1000$ GeV).

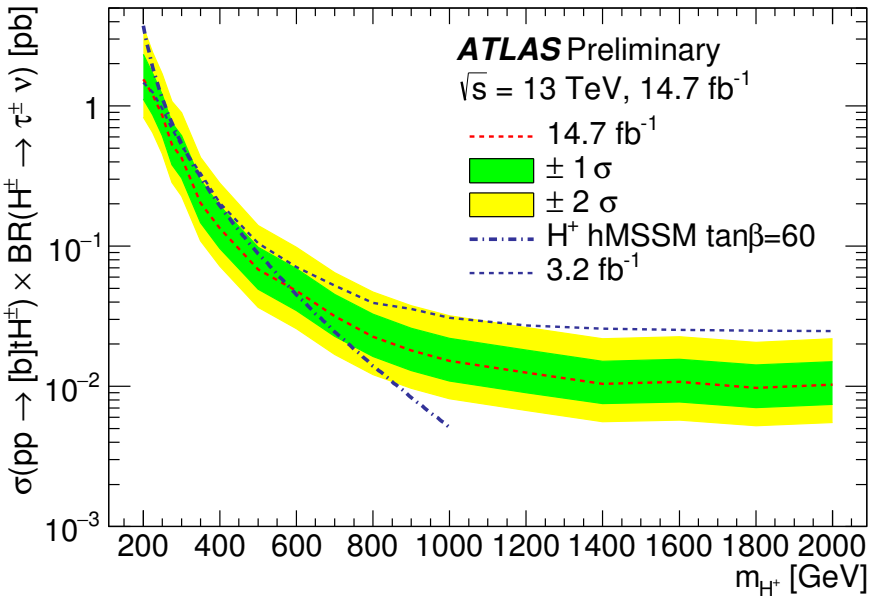

Figure 9: Comparison of the expected 95% CL exclusion limits for heavy charged Higgs boson production as a function of m_{H^+} in 14.7 fb^{-1} of $\sqrt{s}$ = 13 TeV pp collision data and in 3.2 fb^{-1} of $\sqrt{s}$ = 13 TeV pp collision data collected in 2015 [21].